KURKI-SUONIO, K., MERISALO, M. & PELTONEN, H. (1979). *Phys. Scr.* **19**, 57–63.
LARSEN, F. K., BROWN, P. J., LEHMANN, M. S. & MERISALO, M. (1982). *Philos. Mag.* B**45**, 31–50.
LARSEN, F. K. & HANSEN, N. K. (1984). *Acta Cryst.* A**40**, 169–179.
LARSEN, F. K., LEHMANN, M. S. & MERISALO, M. (1980). *Acta Cryst.* A**36**, 159–163.
MERISALO, M., JÄRVINEN, M. & KURITTU, J. (1978). *Phys. Scr.* **17**, 23–25.
MERISALO, M. & LARSEN, F. K. (1977). *Acta Cryst.* A**33**, 351–354.
MERISALO, M. & LARSEN, F. K. (1979). *Acta Cryst.* A**35**, 325–327.
SAKATA, M., MORI, S., KUMAZAWA, S., TAKATA, M. & TORAYA, H. (1990). *J. Appl. Cryst.* **23**, 526–534.
SAKATA, M. & SATO, M. (1990). *Acta Cryst.* A**46**, 263–270.
SAKATA, M., TAKATA, M., KUBOTA, Y., UNO, T., KUMAZAWA, S. & HOWARD, C. J. (1992). *Adv. X-ray Anal.* **35**, 77–83.
SAKATA, M., TAKATA, M., OSHIZUMI, H., GOTO, A. & HONDOH, T. (1992). *Physics and Chemistry of Ice*, pp. 62–68. Hokkaido Univ. Press, Sappolo, Japan.
SAKATA, M., UNO, T., TAKATA, M. & HOWARD, C. J. (1993). *J. Appl. Cryst.* **26**, 159–165.
SAKATA, M., UNO, T., TAKATA, M. & MORI, R. (1992). *Acta Cryst.* A**39**, 47–60.
TAKATA, M., KUBOTA, Y. & SAKATA, M. (1993). *Z. Naturforsch. Teil A*, **48**, 75–80.
TAKATA, M., YAMADA, M., KUBOTA, Y. & SAKATA, M. (1992). *Adv. X-ray Anal.* **35**, 85–90.
WILLIS, B. T. M. & PRYOR, A. W. (1975). *Thermal Vibrations in Crystallography*. Cambridge Univ. Press.

Acta Cryst. (1994). A**50**, 337–342

Comparison between Experimental and Theoretical Rocking Curves in Extremely Asymmetric Bragg Cases of X-ray Diffraction

BY SHIGERU KIMURA* AND JIMPEI HARADA

Department of Applied Physics, Nagoya University, Chikusa-ku, Nagoya 464-01, *Japan*

AND TETSUYA ISHIKAWA

Department of Applied Physics, University of Tokyo, 7-3-1 *Hongo, Bunkyo-ku, Tokyo* 113, *Japan*

(*Received* 1 *July* 1993; *accepted* 19 *October* 1993)

Abstract

Double-crystal rocking curves from a highly perfect silicon crystal were taken in extremely asymmetric schemes, in which the glancing angles of the incident X-rays were very close to the critical angle of total external reflection. The experimental rocking curves were compared with theoretical calculations based both on an ordinary dynamical theory of diffraction and also on an extended dynamical theory, which uses a more exact solution of the fundamental equation of the dynamical theory and takes the effect of specular reflection into account. It is demonstrated from such a comparison that, in the case of extremely asymmetric diffraction, the ordinary treatment of the dynamical theory of diffraction is not valid; in contrast, the extended theory explains the rocking curve very well.

1. Introdution

Extremely asymmetric Bragg-case diffraction with an incident-beam glancing angle close to the critical angle of total reflection has been a subject of great interest in applications such as the study of surfaces (Kitano, Ishikawa, Matsui, Akimoto, Mizuki & Kawase, 1987; Kitano, Kimura & Ishikawa, 1992; Kimura, Mizuki, Matsui & Ishikawa, 1992) and interfaces (Hasegawa, Akimoto, Tsukiji, Kubota & Ishitani, 1993). Under these conditions, however, ordinary treatments of the dynamical theory of diffraction (Zachariasen, 1945) are not valid, since the effects of specular reflection can no longer be neglected. Consequently, several theoretical studies (Kishino & Kohra, 1971; Bedyńska, 1973; Rustichelli, 1975; Zeilinger & Beatty, 1983; Afanas'ev & Melikyan, 1990) have been reported on diffraction phenomena in such an extremely asymmetric case. According to the work of these authors: (1) the angular deviation from Bragg's law, $\Delta\theta_0$, approaches the critical angle of total reflection, θ_c, as $\theta_B - \alpha$ goes to zero, where θ_B is the Bragg angle and α is the angle between the crystal surface and diffracting planes; (2) the full width at half-maximum (FWHM) of the rocking curve has a maximum value at a small glancing angle and cannot be larger than this maximum value as $\theta_B - \alpha$ becomes even smaller. The ordinary treatment of the dynamical theory, however, shows that both $\Delta\theta_0$ and the FWHM diverge.

* Permanent address: Microelectronics Research Laboratories, NEC Corporation, 34 Miyukigaoka, Tsukuba, Ibaraki 305, Japan.

Although all the theoretical predictions are consistent, there have been only a few reported experiments on $\Delta\theta_0$ (Brümmer, Höche & Nieber, 1976*a*,*b*) and none on the FWHM. This is because of the difficulty associated with adjusting $\theta_B - \alpha$ within the accuracy of a few tens of arc s in the case of a fixed-wavelength experiment with characteristic X-rays such as Cu $K\alpha_1$ radiation. This means that α should be adjusted with the accuracy of a few tens of arc s.

Recently, Kimura *et al.* (1992) examined the possibility of measuring $\Delta\theta_0$ by changing the wavelength instead of α. With the wavelength tunability of synchrotron radiation, it is relatively easy to adjust $\theta_B - \alpha$. However, since the X-ray optics were arranged in an $(m, -n)$ non-parallel setting, the effects of dispersion hindered the determination of accurate rocking curves, so the FWHM was not obtainable. In the present work, an $(n, -n)$ parallel setting has been employed so that the FWHM is also obtainable. The intensity of extremely asymmetric diffraction from an Si(001) crystal has been measured around three glancing angles by changing the wavelength. Furthermore, we have compared these results with theoretical calculations based on the formulation first presented by Kishino & Kohra (1971) (hereinafter referred to as the extended theory) and also on the ordinary dynamical theory for absorbing crystals (Zachariasen, 1945). The calculation of the extended theory is shown to be clearly superior for the case of extremely asymmetric diffraction.

2. The extended theory of dynamical diffraction

In this section, we present a review of the extended theory, which consists of a more exact solution of the fundamental equation of dynamical theory and also takes the effect of specular reflection into account. Here, only σ polarization is considered because synchrotron radiation is used in the present experiment. The fundamental equations for the two-beam case are

$$[(\mathbf{k}_0^2 - k^2)/\mathbf{k}_0^2]D_0 = \chi_{\bar{h}} D_h \tag{1}$$

and

$$[(\mathbf{k}_h^2 - k^2)/\mathbf{k}_h^2]D_h = \chi_h D_0, \tag{2}$$

where D_0 and D_h are the amplitudes of the waves inside the crystal, which have wave vectors $\mathbf{k}_0$ and $\mathbf{k}_h$, respectively (with the relation $\mathbf{k}_h = \mathbf{k}_0 + \mathbf{h}$, where $\mathbf{h}$ is the reciprocal-lattice vector).

Also, $k^2 = K^2/(1 - \chi_0)$, where K is the wave number in vacuum and χ_0, χ_h and $\chi_{\bar{h}}$ are 4π times the zeroth, hth and $\bar{h}$th Fourier components of the susceptibility of the crystal, respectively. The wave vectors $\mathbf{k}_0$ and $\mathbf{k}_h$ must satisfy the secular equation of (1) and (2); thus, we have

$$[(\mathbf{k}_0^2 - k^2)/\mathbf{k}_0^2][(\mathbf{k}_h^2 - k^2)/\mathbf{k}_h^2] = \chi_h \chi_{\bar{h}}. \tag{3}$$

Rewriting (3) using the relations $|\mathbf{k}_h| = k_h$ and $|\mathbf{k}_0| = k_0$ results in

$$(k_0^2 - k^2)(k_h^2 - k^2) = \chi_h \chi_{\bar{h}} k_0^2 k_h^2. \tag{4}$$

Although Kishino & Kohra (1971) approximated the last two factors, $k_0^2 k_h^2$, on the right-hand side of (4) as k^4, we do not, since we would like to make as few approximations as possible to obtain a more exact solution. Equation (4) shows the dispersion surface, which describes the positions of the origin points of wave vectors $\mathbf{k}_0$ and $\mathbf{k}_h$ in the reciprocal-lattice space, as shown in Fig. 1. Because of the tangential continuity of the incident vacuum wave vector and $\mathbf{k}_0$, (4) is rewritten in terms of the components of these wave vectors normal to surface as

$$\begin{aligned}(K^2\gamma_0'^2 - K^2\Gamma_0^{(i)2})(K^2\gamma_h'^2 - K^2\Gamma_h^{(i)2}) \\ = \chi_h\chi_{\bar{h}}(K^2\cos^2\theta_0 + K^2\Gamma_0^{(i)2}) \\ \times [(K\cos\theta_0 - h\sin\alpha)^2 + K^2\Gamma_h^{(i)2}],\end{aligned} \tag{5}$$

where

$$\Gamma_0^{(i)} = (\mathbf{k}_0^{(i)}\cdot\mathbf{n}/K) = \gamma'_0 - \delta_0, \tag{6}$$

$$\Gamma_h^{(i)} = -(\mathbf{k}_h^{(i)}\cdot\mathbf{n}/K) = (h\cos\alpha/K) - \Gamma_0^{(i)}, \tag{7}$$

$$\gamma_0'^2 = (k^2 - K^2\cos^2\theta_0)/K^2 \tag{8}$$

and

$$\gamma_h'^2 = [k^2 - (K\cos\theta_0 - h\sin\alpha)^2]/K^2, \tag{9}$$

in which δ_0 is an unknown factor corresponding to the resonance error in the conventional treatment and $\mathbf{n}$ denotes a unit vector pointing perpendicular to the surface (inward direction). Also, $h = |\mathbf{h}|$ and α is the angle between the crystal surface and diffracting planes. With (7), (8) and (9), (5) is written in terms of $\Gamma_0^{(i)}$ as

$$\begin{aligned}&\Gamma_0^{(i)4}(1 - \chi_h\chi_{\bar{h}}) + \Gamma_0^{(i)3}[-(2h\cos\alpha/K)(1 - \chi_h\chi_{\bar{h}})] \\ &+ \Gamma_0^{(i)2}\{-\gamma_0'^2 - \gamma_h'^2 + (h\cos\alpha/K)^2 \\ &- \chi_h\chi_{\bar{h}}[2\cos^2\theta_0 - (2h\cos\theta_0\sin\alpha/K) + (h^2/K^2)]\} \\ &+ \Gamma_0^{(i)}[(2h\cos\alpha/K)(\gamma_0'^2 + \chi_h\chi_{\bar{h}}\cos^2\theta_0)] \\ &+ \gamma_0'^2\gamma_h'^2 - \gamma_0'^2(h\cos\alpha/K)^2 \\ &- \chi_h\chi_{\bar{h}}\cos^2\theta_0[\cos^2\theta_0 \\ &- (2h\cos\theta_0\sin\alpha/K) + (h^2/K^2)] = 0.\end{aligned} \tag{10}$$

The four solutions $\Gamma_0^{(i)}$ $(i = 1, 2, 3, 4)$ of (10), which determine the positions of tie points A_1, A_2, A_3 and A_4, as shown in Fig. 1, are numerically obtained. Designation of the index $i = 1, 2, 3, 4$ is made according to

$$\text{Im}\,\Gamma_0^{(1)},\ \text{Im}\,\Gamma_0^{(4)} < 0, \tag{11}$$

$$\text{Im}\,\Gamma_0^{(2)},\ \text{Im}\,\Gamma_0^{(3)} > 0, \tag{12}$$

$$|\mathrm{Re}\, \Gamma_0^{(1)}| < |\mathrm{Re}\, \Gamma_0^{(4)}| \quad (13)$$

and

$$|\mathrm{Re}\, \Gamma_0^{(2)}| < |\mathrm{Re}\, \Gamma_0^{(3)}|. \quad (14)$$

The boundary conditions for the electric-field vectors and magnetic-field vectors must be used as proposed by Kishino & Kohra (1971). If we represent the amplitudes of the incident beam, the specularly reflected beam and the diffracted beam as E_0, E_m and E_h, respectively, then the two sets of boundary conditions at the entrance surface are given as

$$E_0 + E_m = D_0^{(1)} + D_0^{(4)}, \quad (15)$$

$$E_h = D_h^{(1)} + D_h^{(4)} \quad (16)$$

and

$$(E_0 - E_m)\mathbf{K}_0\cdot\mathbf{n} = K\Gamma_0^{(1)}D_0^{(1)} + K\Gamma_0^{(4)}D_0^{(4)}, \quad (17)$$

$$E_h\mathbf{K}_h\cdot\mathbf{n} = K\Gamma_h^{(1)}D_h^{(1)} + K\Gamma_h^{(4)}D_h^{(4)}. \quad (18)$$

Note that $\Gamma_h^{(4)}$ is nearly equal to $-\gamma_h'$ and $D_o^{(4)}$ is nearly zero because $k_0^{(4)} > k$. From (1), (6) and (8), the amplitude ratio $c^{(i)} = D_h^{(i)}/D_0^{(i)}$ is found to be

$$c^{(i)} = (\Gamma_0{}^{(i)2} - \gamma_0{}'^2)/[\chi_{\bar{h}}(\cos^2\theta_0 + \Gamma_0{}^{(i)2})]. \quad (19)$$

From (15)–(19) and (10), the reflectivities of the specularly reflected beam, R_{mirror}, and of the diffracted beam, R_{Bragg}, are given by

$$R_{\mathrm{mirror}} = |E_m/E_0|^2 = |(\sin\theta_0 - \Gamma_0^{(1)})/(\sin\theta_0 + \Gamma_0^{(1)})|^2 \quad (20)$$

and

$$\begin{aligned} R_{\mathrm{Bragg}} &= (|\mathbf{K}_h\cdot\mathbf{n}|/\mathbf{K}_0\cdot\mathbf{n})|E_h/E_0|^2 \\ &= [\sin(\theta_0 + 2\alpha)/\sin\theta_0] \\ &\quad \times |\{(\Gamma_h^{(1)} + \gamma'_h)/[\sin(\theta_0 + 2\alpha) + \gamma'_h]\} \\ &\quad \times [2\sin\theta_0/\sin(\theta_0 + \Gamma_0^{(1)})] \\ &\quad \times [(\Gamma_0^{(1)2} - \gamma_0'^2)/\chi_{\bar{h}}(\cos^2\theta_0 + \Gamma_0^{(1)2})]|^2. \end{aligned} \quad (21)$$

From (21), the rocking curves can be calculated on the basis of the extended theory.

3. Experimental procedure

The experimental arrangement, set up on beam line 15C of the Photon Factory, KEK, Tsukuba, is schematically shown in Fig. 2. The wavelength of the X-rays can be tuned by a fixed-exit double-crystal monochromator of flat Si(111) crystals (Matsushita, Ishikawa & Oyanagi, 1986). The X-rays are collimated by an Si(111) crystal using a 555 symmetric reflection. An Si(001) crystal sample is aligned to give a 555 asymmetric reflection with $\alpha = 54.75°$. This is an $(n, -n)$ non-dispersive setting. A highly perfect silicon wafer of thickness about 8 mm, grown by the floating-zone method, was used for the sample in order to minimize the influence of imperfections and/or impurities in the bulk crystal. Both surfaces were chemically etched to remove the mechanically

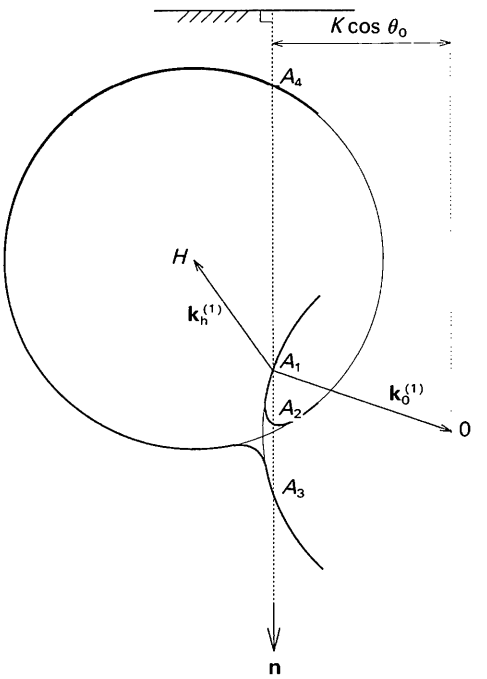

Fig. 1. Dispersion surface, which describes the positions of the origin points of wave vectors $\mathbf{k}_0$ and $\mathbf{k}_h$ in the reciprocal-lattice space, and tie points A_1, A_2, A_3 and A_4.

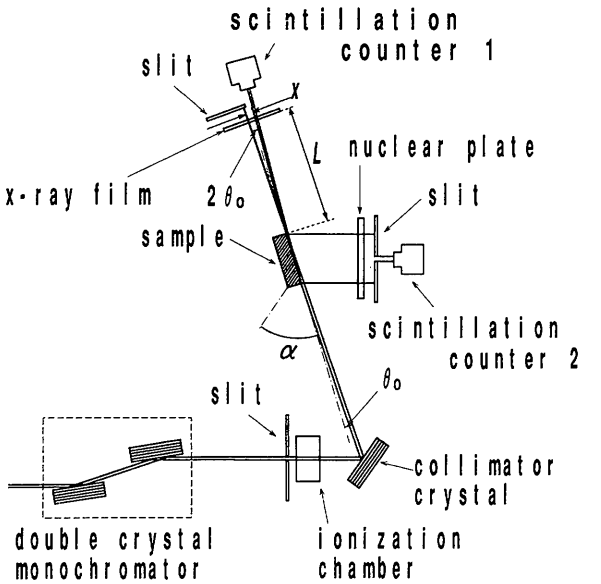

Fig. 2. Schematic diagram of the experimental arrangement set-up on beam line 15C of the Photon Factory. Here α, θ_0, L and x represent the angle between the sample surface and the diffraction plane, the glancing angle to the sample surface, the distance between the sample edge and the X-ray film and the distance between the direct X-ray beam and the specularly reflected X-ray beam on the X-ray film, respectively.

damaged layers left over from the cutting of the wafer from the silicon ingot and then finished by mechano-chemical polishing.

Using the double-crystal monochromator, we can change wavelength with relative precision of about 0.00005 Å because the minimum angular step of the monochromator is 0.5×10^{-3}° (monitored by a rotary encoder). With this tunability, θ_0 can be set near θ_c, where θ_0 is determined by

$$\theta_0 = \tfrac{1}{2} \arctan (x/L), \qquad (22)$$

where x and L are the distances between the direct X-ray beam and the specularly reflected X-ray beam on the X-ray film and between the sample edge and the X-ray film, respectively.

Double-crystal rocking curves were taken for the 555 reflection with 0.2″ step size at the three wavelength values that give the diffraction peaks at glancing angles 9′ 18.3″, 9′ 43.2″ and 10′ 43.7″ (θ_c = 8′ 56.3″). Measurement times were 5 s for each point while the storage ring was operating at an energy of 2.5 GeV with an average positron beam current of 300 mA.

4. Results and discussion

Figs. 3(*a*), (*b*) and (*c*) show the experimental rocking curves, which were obtained around glancing angles of (*a*) 10′ 43.7″, (*b*) 9′ 43.2″ and (*c*) 9′ 18.3″ and $\Delta\omega$ represents the offset angle from the diffraction peak angle. In each figure, a smooth background was subtracted but the angular divergence of the incident X-rays from the collimator crystal was not corrected. The FWHMs of these rocking curves are (*a*) 7.6″, (*b*) 7.4″ and (*c*) 7.0″. In these figures, solid curves represent theoretical rocking curves calculated using the extended theory and dotted curves represent those calculated using the ordinary dynamical theory for absorbing crystals. These were calculated for X-ray wavelengths of (*a*) 1.02485, (*b*) 1.02431 and (*c*) 1.02399 Å, corresponding to the experimental conditions. We used a lattice parameter of 5.43100 Å, a Debye parameter of 0.45 Å^2 and the values of χ_0 and χ_h listed in Table 1, which were estimated using the normal scattering factor (Maslen, Fox & O'Keefe, 1992) and the anomalous scattering factors (Sasaki, 1989). The calculations based on the extended theory show very good agreement with experiment, while the calculation based on the ordinary treatment is clearly incorrect. In case (*c*), the disagreement between the two treatments is especially large. The ordinary treatment fails completely to give a peak diffraction pattern, because the refraction of the incident beam is not properly taken into account. These results clearly show that, in the case of extremely asymmetric diffraction conditions, the ordinary treatment is not valid, while the extended

Table 1. *Values of* χ_0 ($=\chi_{0r} + i\chi_{0i}$) *and* χ_h ($=\chi_{hr} + i\chi_{hi}$) *for the curves in Fig.* 3

λ (Å)	χ_{0r} ($\times 10^{-6}$)	χ_{0i} ($\times 10^{-8}$)	χ_{hr} ($\times 10^{-7}$)	χ_{hi} ($\times 10^{-8}$)
1.02485	−6.65183	−6.96330	−9.72380	−3.69885
1.02431	−6.64482	−6.95596	−9.71356	−3.69495
1.02399	−6.64067	−6.95162	−9.70749	−3.69264

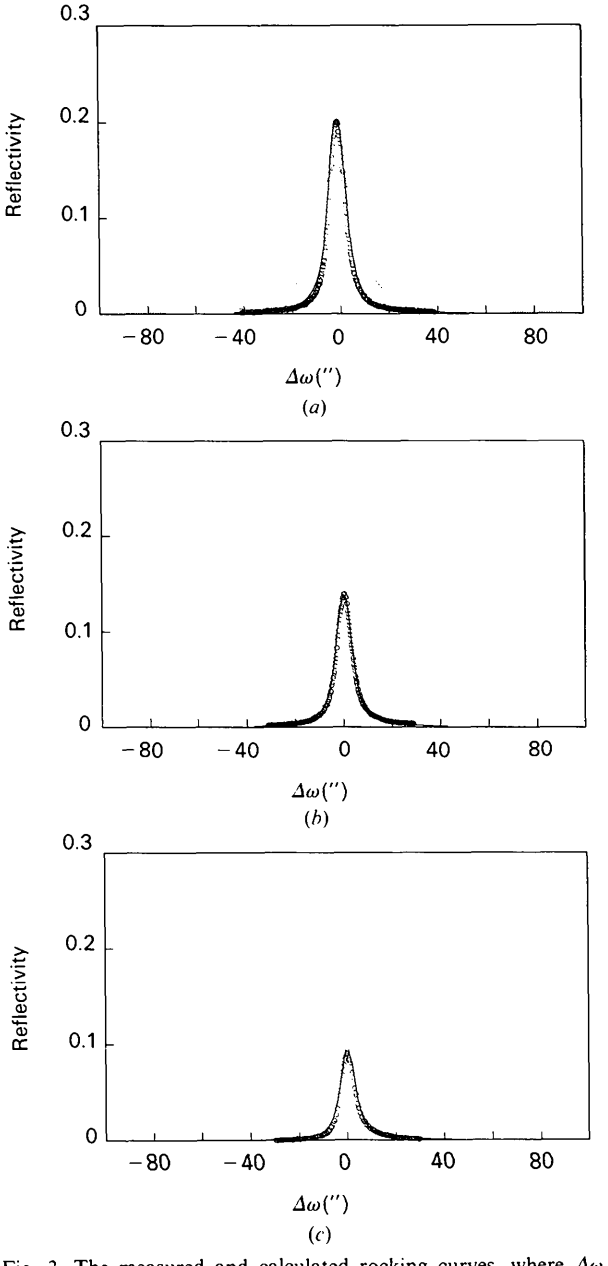

Fig. 3. The measured and calculated rocking curves, where $\Delta\omega$ represents the offset angle from the diffraction peak angle. Open circles represent intensity measured around the glancing angles of (*a*) 10′ 43.7″, (*b*) 9′ 43.2″ and (*c*) 9′ 18.3″, respectively. Theoretical rocking curves calculated for X-ray wavelengths of (*a*) 1.02485, (*b*) 1.02431 and (*c*) 1.02399 Å, respectively, are also shown for the extended theory (solid line) and ordinary dynamical theory for absorbing crystals (dotted line).

theory explains the rocking curves very well. Kishino & Kohra (1971) have predicted theoretically that the FWHM of the rocking curve should have a maximum at a small glancing angle and cannot be larger than this maximum even if the glancing angle becomes smaller. On the other hand, if we follow the ordinary treatment of dynamical theory, the FWHM diverges when the glancing angle tends to zero. This is the first experiment to prove the theoretical prediction of Kishino & Kohra.

A closer examination of Figs. 3(*a*), (*b*) and (*c*) shows that the FWHM of each experimental rocking curve is slightly narrower than that calculated by the extended theory. In the general Bragg case, it is known that a similar tendency is observed by an increase in the thermal vibration of the atoms (Kohra, Kikuta & Annaka, 1965) and/or the presence of randomly distributed impurities (Kikuta & Kohra, 1966) or microdefects (Dederichs, 1971), the effect of which appears in the form of a Debye–Waller factor. Since the penetration depth of the incident X-rays is very shallow in the present case, the narrowing of the peaks must be caused by similar phenomena in the near-surface region. Two possibilities are considered. The first is thermal vibration of the atoms in the near-surface region, which is expected to be larger than that of the bulk crystal. The second is the existence of randomly distributed microdefects in the near-surface region because the effect of these is given in the form of the so-called static Debye–Waller factor (Kato, 1980).

To distinguish between the two possibilities, X-ray topographs were taken with the nuclear plate located in the diffracted beam, as illustrated in Fig. 2. Figs. 4(*a*) and (*b*) show the topographs, which were taken at the glancing angles of (*a*) 10′ 43.7″, corresponding to the experimental condition for Fig. 3(*a*), and (*b*) 13′ 43.4″. Both topographs reveal strain images that cannot be observed by usual X-ray topography. By comparing these two topographs, however, we find that the images are clearer in Fig. 4(*a*) than in Fig. 4(*b*), indicating that these are surface features, because the penetration depth decreases as the glancing angle becomes smaller. We think these images come from strains produced by the polishing pad during mechano-chemical polishing, which is the final step in the manufacturing polishing process of a silicon surface (Kimura *et al.*, 1992). This result supports the second of the possibilities described above, *i.e.* lattice irregularity in the near-surface region causes the slight narrowing of the experimental rocking curves by producing a static Debye–Waller factor. However, it is impossible to deny the first possibility solely from this result.

As presented in this paper, it is essential to use the $(n, -n)$ arrangement in order to measure the very weak signals in extremely asymmetric diffraction conditions. Furthermore, it should be noted that this experiment cannot be carried out without good use being made of synchrotron radiation (*e.g.* high brilliance and wavelength tunability) and also a high-precision diffractometer for multiple-crystal work (Ishikawa, Matsui & Kitano, 1986).

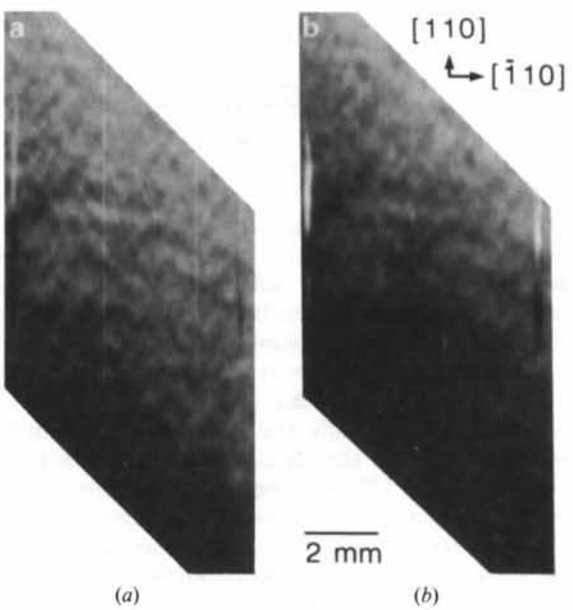

Fig. 4. Topographs of the sample taken at glancing angles of (*a*) 10′ 43.7″ and (*b*) 13′ 43.4″. Exposure times were about (*a*) 4 h and (*b*) 1 h using a nuclear emulsion plate (Ilford L4), placed as indicated in Fig. 2. Misty strain images come from lattice irregularity in the near-surface region produced by mechano-chemical polishing.

The authors thank D. Tweet, K. Akimoto, H. Ono and J. Matsui for helpful discussions and Y. Matsumoto, K. Okada and H. Watanabe for their encouragement. They also thank A. W. Stevenson for his critical reading of the manuscript. This work was performed using synchrotron radiation at the Photon Factory, National Laboratory for High Energy Physics, under a joint research program between the Photon Factory and NEC Corporation.

References

AFANAS'EV, A. M. & MELIKYAN, O. G. (1990). *Phys. Status Solidi A*, **122**, 459–468.

BEDYŃSKA, T. (1973). *Phys. Status Solidi A*, **19**, 365–372.

BRÜMMER, O., HÖCHE, H. R. & NIEBER, J. (1976*a*). *Phys. Status Solidi A*, **33**, 587–593.

BRÜMMER, O., HÖCHE, H. R. & NEIBER, J. (1976*b*). *Phys. Status Solidi A*, **37**, 529–532.

DEDERICHS, P. H. (1971). *Phys. Rev. B.* **4**, 1041–1050.

HASEGAWA, E., AKIMOTO, K., TSUKIJI, M., KUBOTA, T. & ISHITANI, A. (1993). *Extended Abstracts of the* 1993 *International Conference on Solid State Devices and Materials*, pp. 86–88. Chiba: The Japan Society of Applied Physics.

ISHIKAWA, T., MATSUI, J. & KITANO, T. (1986). *Nucl. Instrum. Methods*, **A246**, 613–616.
KATO, N. (1980). *Acta Cryst.* A**36**, 763–769, 770–778.
KIKUTA, S. & KOHRA, K. (1966). *J. Phys. Soc. Jpn*, **21**, 1449.
KIMURA, S., MIZUKI, J., MATSUI, J. & ISHIKAWA, T. (1992). *Appl. Phys. Lett.* **60**, 2604–2606.
KISHINO, S. & KOHRA, K. (1971). *Jpn. J. Appl. Phys.* **10**, 551–557.
KITANO, T., ISHIKAWA, T., MATSUI, J., AKIMOTO, K., MIZUKI, J. & KAWASE, Y. (1987). *Jpn. J. Appl. Phys.* **26**, L108–L110.
KITANO, T., KIMURA, S. & ISHIKAWA, T. (1992). *Appl. Phys. Lett.* **60**, 177–179.
KOHRA, K., KIKUTA, S. & ANNAKA, S. (1965). *J. Phys. Soc. Jpn*, **20**, 1964–1965.
MASLEN, E. N., FOX, A. G. & O'KEEFE, M. A. (1992). *International Tables for Crystallography*, Vol. C, edited by A. J. C. WILSON, pp. 476–516. Dordrecht: Kluwer Academic Publishers.
MATSUSHITA, T., ISHIKAWA, T. & OYANAGI, H. (1986). *Nucl. Instrum. Methods*, A**246**, 377–379.
RUSTICHELLI, F. (1975). *Philos. Mag.* **31**, 1–12.
SASAKI, S. (1989). *Numerical Tables of Anomalous Scattering Factors Calculated by the Cromer and Liberman Method.* KEK Report 88-14. National Laboratory for High Energy Physics, Japan.
ZACHARIASEN, W. H. (1945). *Theory of X-ray Diffraction in Crystals.* New York: John Wiley.
ZEILINGER, A. & BEATTY, T. J. (1983). *Phys. Rev. B*, **15**, 7239–7250.

Acta Cryst. (1994). A**50**, 342–344

Direct Phase Determination for Macromolecular Crystals Using the Multiple-Diffraction Technique and an In-House X-ray Source

BY MAU-TZAI HUANG, CHIEN-MEI WANG AND SHIH-LIN CHANG

Department of Physics, National Tsing Hua University, Hsinchu, Taiwan 30043

(*Received* 10 *June* 1993; *accepted* 25 *October* 1993)

Abstract

This paper reports the first attempt at using a rotating-anode X-ray source and the multibeam diffraction technique to determine the phases of X-ray reflections from macromolecular crystals. Invariant phases of structure-factor triplets of lysozyme are determined unambiguously *via* four-beam diffractions.

Introduction

The determination of triplet-invariant phases of macromolecular crystals using X-ray multiple diffraction has been demonstrated with synchrotron radiation (Hümmer, Schwegle & Weckert, 1991; Chang, King, Huang & Gao, 1991; Hümmer, Schwegle & Weckert, 1992). It is, however, generally believed that conventional laboratory X-ray sources may not be suitable for obtaining intensity profiles with multiple diffraction and for revealing the phase effect from the multibeam interaction in macromolecular crystals because the low photon flux of the sources gives weak signals and counting statistics, the poor degree of beam parallelism makes coherent interaction of X-ray wavefields difficult and the untunable wavelength provides no way of avoiding peak overlapping. In this communication, we report efforts towards overcoming these difficulties, success in the detection of multiple diffraction profiles from lysozyme using a conventional X-ray source and the results of quantitative determination of the invariant phases associated with the multibeam cases studied.

Experimental

Multiple-diffraction experiments were carried out on a four-circle diffractometer (Huber 5042) with a rotating-anode generator (Elliott, GX-21). A hen egg-white lysozyme crystal ($a = b = 78.9$, $c = 38.1$ Å, tetragonal, space group $P4_32_12$) was first aligned for a primary reflection **G** and then rotated (ψ rotation) around the reciprocal-lattice vector **g** of the **G** reflection to bring secondary reflections **L** and **M** into position to diffract simultaneously the incident beam. The intensity variation of the primary reflection during the ψ scan is recorded as the multiple-diffraction profile. In order to increase the visibility of this diffraction profile and to improve the angular resolution, we let the direct beam go through a collimation pipe 120 cm long with a pinhole 0.3 mm in diameter at its exit, so that the incident beam hit the crystal sample directly and the beam divergences were 0.04° vertically and horizontally for a point source 0.1 × 0.1 mm from a copper target. A nickel filter was used. In addition, we chose strong four-beam diffractions with intensities at least one order of magnitude higher than the adjacent multiple diffractions, according to intensity calculations based on the kinematical theory (see Moon & Shull, 1964).

ISSN 0108-7673